Evolution of coal-bed methane in Southeast Qinshui Basin, China: Insights from stable and noble gas isotopes

Biying Chen[1*], Finlay M. Stuart[1], Sheng Xu[1,2], Domokos Györe[1] and Congqiang Liu[2]

[1]Scottish Universities Environmental Research Centre (SUERC), East Kilbride, G75 0QF, UK

[2]Institute of Surface-Earth System Science, Tianjin University, Tianjin 300072, China

*Author for correspondence: b.chen.1@research.gla.ac.uk

Abstract

The late Carboniferous-early Permian coal seams of the Qinshui Basin in Shanxi Province are the most prolific producer of coalbed methane (CBM) in China. Methane formed in the late Triassic during deep burial and reheating in late Jurassic-early Cretaceous driven by magmatic underplating. Basin inversion brought the coal seams to 400-700 m from the surface in the mid-late Cenozoic. Here we present results of a study aimed at understanding the origin of the methane, and how it was affected by Cenozoic exhumation of the basin. Methane from a 12 km traverse perpendicular to the basin margin in the southeast part of the basin have stable isotope compositions ($\delta^{13}C$ = -30.2 to -35.2‰, and δD = -155 to -194‰) indicating a thermogenic origin with limited biogenic input. They are, however, lighter than expected based on coal maturity, and $C_1/(C_2+C_3)$ (>1000) are significantly higher than typical thermogenic methane (<50). This is due to diffusive fractionation during commercial gas extraction. He-Ne-Ar isotopes are a mixture of crustal-radiogenic gas with air-derived noble gases. ^4He concentrations (0.52 to 33.25 ppmv) and $^4He/^{40}Ar^*$ ratios (0.06-1.74) are unusually low. He-Ne-Ar concentrations are consistent with the open system Rayleigh fractionation of noble gases derived from air-saturated water with $^4He/^{40}Ar^*$ = 1 during gas extraction. The low $^4He/^{40}Ar^*$, compared with average crust (5) or local production (13) values, implies that more than 90% of the radiogenic ^4He produced in the coals has been lost prior to equilibrium between gas and water phase in the reservoir. This likely occurred in response to gas loss process during rapid exhumation in Cenozoic, showing that the He and Ar content of natural gases is a sensitive indicator of gas loss event caused by recent basin inversion. The event may have led to the loss of up to 44% of the methane from the coal seams. This study demonstrates the importance of basin inversion on gas preservation in shallow CBM, and shows that, in contrast to $\delta^{13}C_{CH4}$, the light noble gases are essential for tracing such a process.

Keywords

Coalbed methane (CBM), Southeast Qinshui basin, noble gas isotopes, gas loss, high coal rank

Highlights

- Gas compositions and stable isotopes indicate diffusive fractionation during commercial gas extraction.
- There is no indication of mantle volatiles in gas samples, no evidence of mantle heating during the Yanshanian Orogeny.
- The low radiogenic He and He/Ar ratio indicate loss of free gas during basin exhumation.

1. Introduction

Coalbed methane (CBM) was first commercially exploited in USA in the late 1970s (Flores, 1998; Golding et al., 2013; Moore, 2012) and accounted for 8-10% of the national natural gas production (Al-Jubori et al., 2009; USEIA, 2013). Australia and China commenced the exploitation of CBM in 1990s, followed by Canada and India (Golding et al., 2013; Moore, 2012). The presence of shallow coalbeds in many parts of the world and the recent developments on horizontal drilling techniques means that CBM can be cheaper to exploit than other conventional onshore and offshore natural gas reservoirs (Golding et al., 2013; Moore, 2012).

Coalbed methane is adsorbed on the coal matrix or absorbed in the micropores (Al-Jubori et al., 2009; Hildenbrand et al., 2012; Rice, 1993). It can be generated by biogenic processes, at the early stage of coalification by methanogens through acetate fermentation or CO_2 reduction (up to 70°C) (Whiticar, 1996), or it can be thermogenic in origin, produced by thermal breakdown of kerogen with increasing temperature and further coalification (>150°C, vitrinite reflectance (R_o) >0.5%) (Clayton, 1991; Strąpoć et al., 2011). The gas yield is suggested to be positively correlated with the coal rank (Moore, 2012; Rice, 1993; Zhang et al., 2008). Generally, the adsorption capability of coal to gas also increases with higher coal rank if all other variables (e.g. coal ash, moistures) are equal (Laxminarayana and Crosdale, 1999; Moore, 2012). The inversion of coal-bearing basins results in a decrease of the reservoir pressure that can induce gas loss by desorption, diffusion and free gas flow (Rice, 1993; Xia and Tang, 2012). Interaction with shallow groundwaters can result in the generation of secondary biogenic methane, the consumption of methane and wet hydrocarbons (C_{2+}) and the dissolution and removal of methane (Qin et al., 2006; Rice, 1993; Strąpoć et al., 2007; Tao et al., 2007).

The stable isotope and major gas compositions of coalbed gases have been used to constrain their origin and accumulation history (Aravena et al., 2003; Flores et al., 2008; Hoşgörmez et al., 2002; Kinnon et al., 2010; Rice, 1993; Strąpoć et al., 2007; Zazzeri et al., 2016; Zhang et al., 2018). The methane is generally accompanied by minor amounts of wet gases, carbon dioxide and nitrogen. CBM is generally deficient in wet gases compared to conventional natural gases (Song et al., 2012). The stable isotope composition of CBM worldwide is highly variable ($\delta^{13}C_{CH4}$ = -83 to -17‰, δD_{CH4} = -415 to -117‰) reflecting the formation mechanism and temperature, and the basin history (Aravena et al., 2003; Flores et al., 2008; Rice, 1993; Song et al., 2012).

The concentration and isotopic composition of the noble gases (He, Ne, Ar, Kr and Xe) in natural gases provide complementary information on gas source and the physical processes that have acted upon them (Ballentine and O'Nions, 1992; Ballentine et al., 1991; Barry et al., 2016; Battani et al., 2000; Byrne et al., 2018; Sherwood Lollar et al., 1997; Torgersen and Kennedy, 1999; Xu et al., 1995; Zartman et al., 1961). They have, however, only been used sparingly in studies of CBM. Zhou et al. (2005) demonstrated that the isotopic and elemental ratios of noble gases fractionate during the gas extraction process in San Juan Basin, and they developed a model on gas-water interaction in the reservoir and its influence on CBM production. The ^{4}He content in CBM gas samples has been used to determine the age of formation waters in reservoirs to constrain the timescale of hydrodynamic processes which have affected hydrocarbon preservation (Zhou and Ballentine, 2006). Györe et al. (2018) argued the influence of external heating on gas generation based on the presence of mantle-derived noble gases in CBM from central Scotland, and the possibility of using high helium concentrations in CBM (100s-1000s ppmv) to monitor gas emission during CBM extraction activities. Noble gases in CBM from Illinois Basin also has been used to identify and quantify the exogenous thermogenic gas in the reservoir, and improve the understanding of the origin of methane in the reservoir (Moore et al., 2018).

The Qinshui Basin is the largest coal bed methane basin in China. It has proven reserve of 4.35×10^{11} m^3 methane and by the end of 2017 it was responsible for more than 70% of Chinese national CBM production (Song et al., 2018). The main commercial CBM extraction focuses on the coal seams in southeast part of the basin (SQB) (Su et al., 2005) where the pore pressure is approximately equal to the hydrostatic pressure (Meng et al., 2011). The coal of the SQB is high rank (vitrinite reflectance, R_o=2.4-4.5%) which is believed to have been the result of a thermal pulse caused by the intrusion of mantle-derived melts in the late Mesozoic (Song et al., 2018; Su et al., 2005). The SQB gases are typically methane-rich (> 95%) (Li et al., 2014; Zhang et al., 2018; Song et al., 2018) with C isotopic compositions that imply a thermogenic origin with only minor contributions of biogenic methane (Li et al., 2014; Su et al., 2005; Zhang et al., 2018; Zhang et al., 2019). The basin exhumed to its current state during the Cenozoic (Cao et al., 2015; Ren et al., 2005; Zeng et al., 1999). The extent to which this affected CBM preservation is poorly understood. Thus, the basin is an ideal natural laboratory to detect the role of recent exhumation to gas migration from the reservoir rocks.

In this study we use the C, H isotopes of methane and noble gas isotope composition of well gases from the SQB to determine the role the late Mesozoic mantle-derived melts may have played in methane generation, and to understanding the extent to which the high coal rank and Cenozoic exhumation have played in accumulation of the CBM.

2. Geological setting

The Qinshui Basin in Shanxi Province, northeast China, is a syncline of Palaeozoic-Mesozoic sediments in the central belt of the North China craton (Figure 1) (Cai et al., 2011; Song et al., 2018; Su et al., 2005; Zhang et al., 2015). Coal deposition started in the Late Carboniferous in response to marine transgression and ended in the Early Permian with fluvial-deltaic sedimentation (Ma et al., 2016; Su et al., 2005). Subsidence continued until the Late Triassic by which time the coal had reached ~135°C (corresponding to more than 4 km depth), inducing the first period of methane generation and maturation of coal to medium volatile bituminous ($R_o \approx 1.2\%$) (Cai et al., 2011; Zeng et al., 1999). The Indosinian orogeny resulted in uplift and basin inversion in the early Jurassic, followed by modest sedimentation until Late Jurassic (Ma et al., 2016; Zeng et al., 1999). Magmatic activity during the Yanshanian orogeny (Late Jurassic to Early Cretaceous) is evident from diorite porphyry bodies that are exposed at the margin of the basin. These are widely accepted to have caused a second peak of gas generation (Ren et al., 2005; Xu et al., 2004; Zeng et al., 1999). Zircon fission track data suggest that temperatures reached over 250°C, which resulted in the conversion of the bituminous coals to semi-anthracite and anthracite with R_o values reaching 2.2-4.5% (Ren et al., 2005; Su et al., 2005). The basin underwent a major phase of exhumation during the Cenozoic that is ultimately related to the extensional tectonic regime induced by the subduction of the Indian Plate in the southwest, or roll back of the subducting Pacific Plate in the east (Cai et al., 2011; Cao et al., 2015). Fission tracks in apatites from sediments overlying coal seams in the SQB reveal that the basin cooled from over 250°C to ~100°C in the last 50 million years then experienced a pulse of rapid cooling to less than 60°C in the last 11 million years (Cao et al., 2015; Ren et al., 2005). Denudation is continued until at least 5 million years (Cao et al., 2015).

The main coal-bearing strata are the 50-135 m thick Pennsylvanian Taiyuan Formation and the 20-40 m thick Early Permian Shanxi Formation (Figure 2) (Su et al., 2005). Coal seam 3 (2-7 m thick) in the Shanxi Formation (R_o=2.5-4.5%) and coal seam 15 (1-6 m thick) in the Taiyuan Formation (R_o=2.7-4.5%) are present across the whole basin and are the most economically important coals (Song et al., 2018; Su et al., 2005). The Taiyuan Formation

coal seams are mostly located at less than 700 m depth, approximately 80 m deeper than the main Shanxi Formation coals. In the study region, a third major coal seam (no. 9) in the Taiyuan Formation, which is about 40 m deeper than coal seam 3, is co-exploited with seams 3 and 15 (Wang et al., 2013).

The main hydrological influence on coal seams is sourced from the confined C_3t aquifer and P_1s-P_1x aquifer (Figure 1D) (Zhang et al., 2015). The no. 9 and 15 coal seams in the Taiyuan Formation are isolated from the underlying aquifer by bauxite and shale in Benxi Formation (Figure 2) (Zhang et al., 2015). The roof of the no. 15 coal seam is a 2-30 km thick limestone, belonging to the C_3t aquifer. The roof and floor of mudstones isolated the no.9 coal seam (Wang et al., 2013). The no. 3 coal seam belongs to P_1s-P_1x aquifer (Zhang et al., 2015). The roof and bottom of the no. 3 coal seam are fine sandstone and mudstone, respectively, which seals the layer as an individual aquifer (Su et al., 2005). The outcrops of the east and south coals in the SQB are the main source of recharging water (Su et al., 2005; Zhang et al., 2015). The groundwater flows northwest and is prevented by a gas and water-sealed fault, Sitou Fault (Su et al., 2005).

3. Sampling and analytical techniques

Nineteen gas samples were taken in April 2017 from wellheads along an E-W transect perpendicular to the boundary fault in the Panzhuang block (Figure 1). This transect is approximately along the groundwater recharge pathway. Seventeen gas samples are from vertical wells, all but one combines the three main coal seams. Well gas Qs19 is from coal seam 15. only. Two gas samples (Qs15 and Qs17) are from horizontal wells within coal seam 15. Well depths vary from 300 to 650 m (Table 1). The wells have been producing methane for between 3 months and 15 years (Table 1).

Samples were collected and stored in Cu tubes at 1.5-2 bar using the method described in Györe et al. (2015). Approximately half of the gas in each tube was used for the determination of the major gas composition and stable isotopes. Gases were expanded into a glass gas-purification system ($p < 0.01$ mbar) and an aliquot was extracted by a 100 μL Hamilton syringe. Major gas composition was determined in nine gas samples by a newly set up Hewlett Packard 5890 gas chromatograph (GC) in SUERC. It is equipped with a single filament thermal conductivity detector, a 2.13 m long, 1.0 mm internal diameter Restek 100/120 packed column operated with helium carrier gas. The temperature of the column during analysis was kept at 30°C for 3 minutes and increased to 150°C at a rate of

15°C/minute and then held at the maximum temperature for 5 minutes. The reproducibility of $CH_4/(C_2H_6 + C_3H_8)$ and CH_4/CO_2 ratios is ±1%.

The carbon isotopic composition was determined using a VG SIRA II dual inlet isotope ratio mass spectrometer (Dunbar et al., 2016) using established procedures in Györe et al. (2018). δC_{CH4} values were determined relative to PDB (Craig, 1957). The hydrogen isotope composition of the water vapour was analysed by a VG Optima dual inlet isotope ratio mass spectrometer (Donnelly et al., 2001). δD_{CH4} values were determined relative to V-SMOW (Gonfiantini, 1978). Experimental uncertainties (1σ) of $\delta^{13}C_{CH4}$ and δD_{CH4} values are ±0.3‰ and ±3‰, respectively.

The remaining gas was used for noble gas analysis using a MAP 215–50 mass spectrometer following procedures described elsewhere (Györe et al., 2015). Blank levels for all isotopes are negligible compared with the signal of samples. Mass spectrometer sensitivity and mass fractionation were determined using the HESJ standard for He (Matsuda et al., 2002), and air (Eberhardt et al., 1965; Györe et al. 2019; Lee et al., 2006; Mark et al., 2011; Ozima and Podosek, 2002) for Ne and Ar. The reproducibility of the absolute concentrations is <4%, and isotopic ratios are less than 1%.

4. Results

Methane is the dominant gas (>95%) in all samples, with minor N_2 and trace CO_2. The wet gases (C_2H_6, C_3H_8) were below detection limit (0.1%) of the GC, which indicates the $CH_4/(C_2H_6 + C_3H_8)$ ratio is higher than 1,000. The CH_4/CO_2 ratio varies from 152 to 806 (Table 1). The carbon and hydrogen isotopic compositions of methane range from -30.2 to -35.2‰ and -155 to -194‰, respectively (Table 1).

^{4}He concentrations range from 0.52 to 33.3 ppmv. $^3He/^4He$ ratios vary from 0.009 ± 0.002 to 0.482 ± 0.007 R_A, where R_A is the atmospheric ratio of 1.34×10^{-6} (Mishima et al., 2018). ^{20}Ne concentrations range from 0.001 to 5.61 ppmv. Neon isotopes appear to be largely air-derived without evident mantle or crustal contribution; $^{20}Ne/^{22}Ne$ and $^{21}Ne/^{22}Ne$ ratios vary from 9.69 ± 0.09 to 10.18 ± 0.03 and from 0.0285 ± 0.0005 to 0.0301 ± 0.0007, respectively. Radiogenic ^{21}Ne is unequivocally present in Qs6, Qs21 and Qs22. ^{40}Ar concentrations range from 23 to 2290 ppmv. $^{40}Ar/^{36}Ar$ range from 291 ± 1 to 497 ± 1, with samples Qs7, Qs 9 and Qs14 having ratios that are lower than the air value (298.6 ± 0.3; Lee et al. (2006); Mark et al. (2011)). $^{38}Ar/^{36}Ar$ ratios are indistinguishable from air (0.1885 ± 0.0003; Lee et al. (2006); Mark et al. (2011)) (Table 2). The gas from coal seam 15 (Qs15, Qs17 and Qs19) is not

evidently distinct from the combined-seam gases in gas compositions, stable isotopes and noble gases.

5. Discussion

5.1. The post-generation fractionation of molecular and stable isotopic compositions

The C, H isotopic compositions (δC_{CH4} = -30.2 to -35.2‰ and δD_{CH4}= -155 to -194‰) of the methane is indicative of a thermogenic origin (Figure 3). However, based on the coal maturity in SQB, the lowest $\delta^{13}C_{CH4}$ value is predicted to be -27‰ (Hu et al., 2001; Li et al., 2014). This is up to 8‰ higher than measured values and hints at modification by other process(es). Stable isotopes of the SQB methane are apparently lighter than reported for methane from other CBM reservoirs of similar maturity (Kotarba and Rice, 2001; Schoell, 1980). Further, C_1/C_{2+} ratios are significantly higher than typical thermogenic gases (<50; Bernard et al. (1976)). The abnormally lighter stable isotopes and high C_1/C_{2+} in SQB have been commonly reported (Chen et al., 2007; Hu et al., 2001; Li et al., 2014; Qin et al., 2006; Zhang et al., 2018).

Similar major gas and methane C isotope values for SQB gases have previously been explained as due to the preferential dissolution of $^{13}CH_4$ and heavy hydrocarbons in groundwater (Li et al., 2014; Qin et al., 2006). However, this is difficult to reconcile. Experimental work has demonstrated that dissolution of methane should result in only small depletion of $\delta^{13}C$ (< -0.5‰) in the free methane phase, and a δD enrichment (< -16‰) that is in the opposite sense to that recorded by the methane (Bacsik et al., 2002).

The addition of secondary biogenic methane has been proposed in several studies to explain the high C_1/C_{2+} and light $\delta^{13}C$ of SQB methane (Chen et al., 2007; Li et al., 2014; Rice, 1993; Zhang et al., 2018). The light $\delta^{13}C_{CH4}$ (up to -61.7‰) of methane desorbed from SQB coal cores supports the addition of biogenic methane. However, fewer than 10% of all SQB samples have $\delta^{13}C_{CH4}$ lighter than -40‰. Using an upper limit of $\delta^{13}C$ = -50‰ for biogenic methane, and $\delta^{13}C$ = -27‰ for thermogenic methane (Li et al., 2014), the methane sampled in this study should be up to 50% biogenic in origin. The factor of two difference in C_1/C_{2+} is not high enough to explain the complete absence of heavy hydrocarbons in most of the SQB gases in this study. Thus, while there may be modest contributions of biogenic methane, it is unlikely to be the key to the ubiquitous high C_1/C_{2+} and light $\delta^{13}C_{CH4}$.

Desorption and diffusion of deep methane to shallow depths during basin exhumation has also been proposed to explain the high C_1/C_{2+} and light $\delta^{13}C_{CH4}$ (Chen et al., 2007; Zhang et

al., 2018; Zhang and Tao, 2000; Zhang et al., 2019). The $\delta^{13}C$ of methane gas desorbed for 4 hours from SQB anthracite is 8‰ lighter than the methane collected after 96 hours of desorption, supporting the hypothesis that light methane readily desorbs at early stages (Zhang and Tao, 2000). The negative trends in $\delta^{13}C_{CH4}$ vs. C_1/C_{2+} and $\delta^{13}C_{CH4}$ vs. C_1/CO_2 (Figure 4A, B) reveal that desorption and diffusion have also caused molecular fractionation as C_{2+} and CO_2 are harder to desorb and diffuse in coalbeds than CH_4 (Bae and Bhatia, 2006; Rice, 1993). However, if isotopically light methane migrates up-seam (Zhang et al., 2019), there should be a positive relationship between coal seam depth and $\delta^{13}C_{CH4}$, C_1/C_{2+} ratio and C_1/CO_2. This is not apparent in this study (Table 1). A positive relationship between $\delta^{13}C_{CH4}$ and gas production rate is evident from the dataset (Figure 4C). This implies that the change of $\delta^{13}C_{CH4}$ has occurred during natural gas extraction. At the early stage of gas extraction, the most easily desorbed gases are produced, and as production continues and the rate of gas production rises, the isotopically heavier CH_4 and the more adsorbent gases (C_{2+}, CO_2) are released (Figure 4).

It is important to note that even when $\delta^{13}C_{CH4}$ approaches the predicted value, the C_1/C_{2+} ratio (> 400) is evidently higher than typical value (< 50) (Figure 4A) (Zhang et al., 2018). Even considering the addition of biogenic methane, the maximum C_1/C_{2+} ratio can only be two times higher (< 100). Ethane and propane are cracked to methane by pyrolysis or the existence of redox couples at temperature in excess of 250°C (Burruss and Laughrey, 2010). The absence of heavy hydrocarbon gases in SQB is thus likely to be the result of cracking of wet gases into methane at high temperature. This is consistent with the detrital zircon fission track thermochronology that indicates such temperatures were attained during the early Cretaceous (Ren et al., 2005). This gives further credence to the idea that the methane generation peak occurred during the Yanshanian Orogeny.

5.2. Identifying the noble gas components

The He and Ne in the SQB gases appear to plot on mixing lines between a deep gas with high He/Ne (> 700)-low $^3He/^4He$ (< 0.03 R_A) and noble gases with composition that can be derived from mass fractionated air (Figure 5A). The five gases with the lowest $^4He/^{20}Ne$ (grey circles in Figure 5A) have air-like $^{40}Ar/^{36}Ar$ ratios and high concentrations of ^{20}Ne and ^{36}Ar (Table 2) that are consistent with being dominated by air-derived noble gases. Both the high and low He/Ne samples have a similar range of ^4He concentrations but the air-rich (low He/Ne) gases have higher ^{20}Ne concentrations (Figure 5B), suggesting that air-derived noble gases have been added to deep gas. As well as fractionated He/Ne (Figure 5A), the five air-

rich samples have Ne isotopes that plot along the mass fractionation line in the $^{20}Ne/^{22}Ne$ vs. $^{21}Ne/^{22}Ne$ space (Figure 6), and three samples have $^{40}Ar/^{36}Ar$ that are lower than air value, also suggestive of fractionation (Table 2). The fractionated air-derived light noble gases may originate in liquids injected during hydraulic fracturing before pumping (Barry et al., 2018) or acquired during the sampling process. It dominates the noble gases of the five low He/Ne samples and these samples are not discussed further.

The high $^{4}He/^{20}Ne$ ratio (37-691) of the remaining samples rules out a significant contribution of air. After correcting the measured $^{3}He/^{4}He$ for minor air-derived He on the basis of the atmospheric He/Ne (0.32), these gases yield values of between 0.008 and 0.035 R_A. This range is typical of crust-derived gases where radiogenic production of ^{4}He occurs by U and Th decay and nucleogenic production of ^{3}He by the reaction $^{6}Li(n,\alpha)^{3}H(\beta^{-})^{3}He$ (Morrison and Pine, 1955). Using the range of Li measured in coal seam 15 (12-78 ppmm, n=12), and the concentration of the large neutron cross-section elements (B, Be, Nd, Gd, etc.) in the Jincheng coals which is the closest coal mine to the study site (Zhang et al., 2004; Zhao, 1997; Zhao et al., 2018), we calculate a $^{3}He/^{4}He$ production ratio of 0.015 to 0.085 R_A (Figure 5A). This covers much of the range measured in the high He/Ne gases. The extremely low $^{3}He/^{4}He$ of samples Qs18 and Qs22 implies that, locally, Li concentrations may be lower, or the concentration of large neutron cross-section elements may be higher.

There is a possibility that the range of $^{3}He/^{4}He$ is due to the presence of a small contribution of mantle-derived He ($^{3}He/^{4}He_{magma}$ = 6-7 R_A; Gautheron and Moreira (2002)) from the early Cretaceous Yanshanian magmatism (Ren et al., 2005; Xu et al., 2004). Using the lowest measured $^{3}He/^{4}He$ (0.008 R_A) as representative of the crustal radiogenic He composition, and 6.1 R_A to represent the magmatic end-member, the highest measured $^{3}He/^{4}He$ requires a maximum mantle He contribution of 0.5%. This is trivial and provides no support for the contention that the main methane generation occurred in response to magmatic heating. Mantle-derived Ne is present in CBM deposits from sedimentary basins that have been intruded by magmatic bodies (e.g. Györe et al. 2018). The absence of mantle-derived Ne in the SQB methane is consistent with the He isotope record.

5.3.Helium loss during Cenozoic exhumation

Compared with other CBM reservoirs of a similar age (e.g., Illinois coals, Moore et al. (2018); Airth coals, Györe et al. (2018)), the ^{4}He concentrations in the high $^{4}He/^{20}Ne$ SQB gases are extremely low (Figure 7A). However, the concentration of radiogenic ^{40}Ar (denoted

as $^{40}Ar^{*}$ and calculated by removing atmospheric ^{40}Ar and assuming negligible magmatic $^{40}Ar^{*}$) in the SQB natural gases overlaps the range recorded by CBM from similar age coals above (Figure. 7B). Consequently, $^{4}He/^{40}Ar^{*}$ ratios (0.06 to 2) in the SQB gases are lower than the average production ratio of the upper continental crust (4.9, Ballentine and Burnard (2002)) or the local coals (> 13), calculated using the lowest U (0.5 ppmm) and Th (0.6 ppmm) (Zhang et al., 2004) and highest K concentration (0.16%, Zhao (1997)).

$^{4}He/^{40}Ar^{*}$ in natural gases are commonly higher than produced in the shallow crust (Ballentine et al., 1994), a function of the low temperature mobility of He relative to Ar. Considering the evident fractionation of C isotope composition and the C_1/C_{2+} ratio of the SQB gases during pumping process, it is reasonable to assume that $^{4}He/^{40}Ar^{*}$ ratio also experienced fractionation during this process. We use the Rayleigh fractionation law (Eq. 1) to test it:

$$(\frac{A}{B})_w = (\frac{A}{B})_o f^{(\alpha-1)} \qquad (1)$$

where $(\frac{A}{B})_w$ is the current elemental ratio in the water phase, $(\frac{A}{B})_o$ is the initial elemental ratio in the water phase, f is the proportion of residue B in the water, and α is the fractionation factor. Assuming the ratio of water to gas volume (V_w/V_g) at each degassing stage is close to zero, the partition of noble gases reaches equilibrium. The elemental ratios of noble gas in gas bubbles can be estimated by Eq.2 :

$$(\frac{A}{B})_g = (\frac{A}{B})_w \alpha \qquad (2)$$

where $(\frac{A}{B})_g$ is the elemental ratio in the gas. Initial $^{20}Ne/^{36}Ar$ = 0.154 in formation water is calculated from ASW equilibrated 10°C at an altitude of 740 m, with 10% Ne excess air (Kipfer et al., 2002; Peeters et al., 2003). The fractionation factor is calculated for the Henry's constants of noble gas and corrected from liquid phase activity coefficients and gas phase fugacity coefficients (Ballentine et al., 2002; Crovetto et al., 1982; Smith and Kennedy, 1983) in groundwater at 27°C and 4 MPa, and salinity of 0.04 mol/L (Wang et al., 2015). If the kinetic diffusion under non-equilibrium condition controls the noble gases partition, the Rayleigh equation is still applicable, only with the fractionation factor proportional to the inverse of the square root of the reduced mass which could be assumed to be equal to the mass of noble gas isotope (Ballentine et al., 2002; Zhou et al., 2005). However, the extent of $^{20}Ne/^{36}Ar$ change for mass-controlled fractionation cannot explain the range observed in the samples (Figure 8). The least air-contaminated SQB gases (i.e. $^{4}He/^{20}Ne$ > 400) plot on a

trend in $^{4}He/^{40}Ar^{*}$-$^{20}Ne/^{36}Ar$ space that is consistent with open system Rayleigh fractionation of gas with $^{20}Ne/^{36}Ar$ of air-saturated water (ASW) based on local conditions (Figure 8). This demonstrates that the radiogenic ^{4}He and ^{40}Ar in the reservoir were dissolved in the formation water and degassed during CBM extraction. Formation water with an initial $^{4}He/^{40}Ar^{*}$ ratio of 13.0 (local production in coals) and 4.9 (average continental crust) provide poor fits to the data. The best fit to the data is derived for an initial $^{4}He/^{40}Ar^{*}$ that approaches a value of 1.0. This implies that the formation water had an abnormally low $^{4}He/^{40}Ar^{*}$ prior to commercial extraction of methane.

The main storage mechanism of gas in coal is by adsorption on the coal matrix or absorption in the micro-pores (Al-Jubori et al., 2009; Hildenbrand et al., 2012; Rice, 1993). The rapid uplift of sedimentary basins induces a drop of reservoir pressure, weakening the sorption capability of coal (Rice, 1993; Xia and Tang, 2012). Adsorbed and absorbed gases are released (desorbed) and accumulate in coal microstructures, generating a pressure gradient that results in gas escape by diffusion or viscous flow (Hildenbrand et al., 2012; Rice, 1993). Gas escape is mainly controlled by the permeability of the coals and pressure gradient between gas phase and wetting phase (Hildenbrand et al., 2012). The rapid Cenozoic inversion of the Qinshui Basin, from over 3 km to ~400 m deep, is likely to have resulted in episodic gas expulsion from the coal seams. A series of detailed gas breakthrough experiments on high rank coals (R_o = 2.3%) from the Qinshui Basin mimicked the effect of over-pressure (Han et al., 2010a). It revealed that at reservoir conditions, He and Ar could escape from wet-coal matrix due to high pressure gradient by mainly diffusion and rarely capillary-viscous flow if macro fractures (e.g. cleats) existed in coalbeds (Han et al., 2010a). They also showed that the effective permeability of He for diffusion is significantly higher than for Ar (Han et al., 2010a). Consequently, during continuous and intensive basin inversion, Ar is likely to have remained trapped in the coalbeds while most of the He lost. Further, the solubility of Ar in water is higher than He (Crovetto et al., 1982; Smith and Kennedy, 1983). Thus the preservation of old formation waters in the SQB (Wang et al., 2018) will tend to have further reduced the $^{4}He/^{40}Ar^{*}$. The loss of He after magmatic events explains that absence of mantle He in the SQB methane.

^{21}Ne excess (denoted as $^{21}Ne^{*}$) in samples is generated by nucleogenic reactions, $^{18}O(\alpha,n)^{21}Ne$ and $^{24}Mg(n,\alpha)^{21}Ne$, in the coals (Yatsevich and Honda, 1997). Only samples Qs6, Qs21 and Qs22 have evident $^{21}Ne^{*}$excess ($9.6 \pm 3.3\times10^{-14}$ to $3.1 \pm 1.6\times10^{-13}$ cm^3 STP/cm^3) beyond analytical uncertainty. It gives the $^{21}Ne^{*}/^{40}Ar^{*}$ ratio of $1.1 \pm 0.6 \times10^{-8}$ to $2.0 \pm 1.0 \times10^{-8}$. The

minimum theoretical local production of $^{21}Ne^{*}/^{40}Ar^{*}$ in SQB is estimated to be 7.8×10^{-8} based on O (5.5%), Mg (0.4%) (Yin et al., 2016; Zhao, 1997) and lowest U, Th concentrations in coals. It is far higher than calculated value in the samples. The absence of crustal-radiogenic or mantle Ne in the samples, demonstrating that most of the non-atmospheric Ne was lost with ^{4}He.

As the He in the SQB well gases has mainly degassed from the coal formation water, the accumulation time of ^{4}He can be estimated (Craig and Lupton, 1976; Torgersen, 1980; Zhou and Ballentine, 2006) from Eq 3 & 4:

$$[He]_{in\ situ} = \frac{\rho \Lambda J(1-\varphi)}{\varphi}\ t \qquad (3)$$

$$J=0.2355\times10^{-12}[U]\{1+0.123([Th]/[U]-4)\} \qquad (4)$$

where $[He]_{in\ situ}$ is the *in situ* production rate in cm^3 STP $^{4}He/(cm^3_{H_2O}\ yr)$, ρ is the density of the coal in g/cm^3, Λ is the fraction of He generated in the coal that enters the pore fluid and assumed to be 1 following Zhou and Ballentine (2006). φ is the porosity of the coal and J is the production rate of ^{4}He in the coal in cm^3 STP $^{4}He/(cm^3_{H_2O}\ yr)$. [U], [Th] are the concentrations in the coal seams in ppmm. Assuming that the coals have density of 1.6 g/cm^3, porosity of 5% (Cai et al., 2011), and all the ^{4}He has been generated in rock with average U and Th concentrations of 3.9 ppmm and 8.5 ppmm, respectively (Zhang et al., 2004), it gives the *in situ* production rate of 1.8×10^{-11} cm^3 STP $^{4}He/(cm^3_{H_2O}\ yr)$ in SQB coals. As He-Ne-Ar follows the open system Rayleigh fractionation, with assumption that the original $^{20}Ne/^{36}Ar$ in formation water is ASW (0.154), the residual ^{36}Ar (*f*) in the formation water can be calculated based on equation 1 and 2, allowing the initial $^{4}He/^{36}Ar$ to be calculated. The initial ^{36}Ar in ASW under local conditions is about 1.3×10^{-6} cm^3 $STP/cm^3_{H_2O}$. The initial concentration of ^{4}He in formation water before fractionation is therefore easily estimated and gives the He accumulation age of between 0.5 and 11 million years, which supports the contention that the majority of He has been lost.

This contrasts with the observed $^{40}Ar^{*}$ concentration. Using the maximum concentration of K (0.16%, Zhao (1997)) and assuming the transfer rate of Ar from rock to fluid of 1, it gives the maximum *in situ* production rate of 1.5×10^{-13} cm^3 STP $^{40}Ar^{*}/(cm^3_{H_2O}\ yr)$. As the solubility of $^{40}Ar^{*}$ and ^{36}Ar is indistinguishable at this scale, the calculated $^{40}Ar^{*}$ concentration in formation water requires 192-1,680 million years, which exceeds the deposition age of coal, and requires the incorporation of the crustal flux of ^{40}Ar flux and/or ^{40}Ar exsolved from

solidifying mantle melts (Castro et al., 1998; Györe et al., 2018; Torgersen et al., 1989). Both of these processes will result in incorporation of ^{4}He in excess of *in situ* production.

Following the method of Zhou and Ballentine (2006), with total thickness of three coal seams to be 8.6 m, we assume that the regional ^{4}He and $^{40}Ar^{*}$ fluxes are 4.9×10^{-8} cm^3 STP $^{4}He/(cm^3_{H_2O}$ yr) and 8.6×10^{-9} cm^3 STP $^{40}Ar^{*}/(cm^3_{H_2O}$ yr), respectively. With both *in situ* and external production, the accumulated age for ^{4}He is $173 - 4\times10^{3}$ yr and $3.3\times10^{3} - 2.9\times10^{4}$ yr for $^{40}Ar^{*}$. The older age defined by $^{40}Ar^{*}$ again supports the contention that He has been most efficiently lost from SQB coals. The $^{40}Ar^{*}$ age overlaps the ^{14}C age of the production water from other regions in SQB ($5\times10^{3} - 4\times10^{4}$ yr) (Wang et al., 2018).

Based on the local $^{4}He/^{40}Ar^{*}$ production rate of 13, the initial $^{4}He/^{40}Ar^{*}$ ratio of 1 before fractionation indicates that over 92% of He has been lost during basin inversion. However, the SQB coals have, obviously, retained economic quantities of methane. This reflects different physical behaviour of CH_4 and the light noble gases. Compared with He and Ar, methane is strongly adsorbed onto the coal and only moves by diffusion in SQB coalbeds (Han et al., 2010a; Han et al., 2010b; Hildenbrand et al., 2012). A model which considers both adsorption/desorption and diffusion during methane loss has been introduced by Xia and Tang (2012). For total organic carbon of 71% (Yin et al., 2016), assuming overpressure of 60 MPa with 250 °C before basin inversion and final conditions of 4 MPa and 27 °C after basin inversion, the free methane concentration decreases from 692 mol/m^3 to 81 mol/m^3, assuming the Peng-Robinson equation of state. The adsorbed gas amount drops from 786 mol/m^3 to 749 mol/m^3 following the Langmuir equation (Xia and Tang, 2012). Considering both the loss of free and adsorbed gas, approximately 44% of the methane has been lost from the SQB during basin inversion. Based on the model in Xia and Tang (2012), the $\delta^{13}C$ of the residue methane would be less than 2‰ heavier than the initial composition. This is contrast with observed lighter $\delta^{13}C_{CH4}$ compared with predicted value. Thus, although the carbon isotope of methane might have been influenced by gas loss event, it has been obscured by later fractionation caused by desorption during gas extraction. This suggests that basin inversion and gas loss are not recorded by stable isotopes (or major gas composition). Although the noble gases experienced open system Rayleigh distillation during gas extraction as well, through modelling, the gas loss could be revealed by light noble gases (He-Ne-Ar). In particular, the radiogenic ^{4}He and $^{40}Ar^{*}$ provide a keen tracer of the timing of gas loss during basin inversion.

6. Conclusion

The stable isotope and major gas composition of CBM from the Qinshui Basin indicates a thermogenic origin with limited biogenic methane. The characteristics have been over-printed by fractionation during gas extraction. The noble gases reveal a mixture of air-derived gases from groundwater (ASW) with deep gases in the reservoir. The mixing of radiogenic ^{4}He and ^{40}Ar and ASW derived noble gases occurred in water phase. Then, they degassed from water following open system Rayleigh fractionation during gas extraction. A gas loss process which happened before the commercial extraction can explain the significantly lower $^{4}He/^{40}Ar^{*}$ in all samples even considering the fractionation process. Meanwhile it also explains the absence of mantle volatiles in the reservoir although the basin was thought to be heated during a magmatic activity in Yanshanian Orogeny (Late Jurassic to Early Cretaceous). The He loss is related to the exhumation of the basin mainly in Cenozoic. Compared with He, Ar, with lower diffusive efficiency and higher solubility, was partly stored in the coal and dissolved in water, which caused the low $^{4}He/^{40}Ar^{*}$ ratio in formation waters. Although about half of the methane also lost during basin inversion, the diagnostic of stable isotopes is weak and easily covered by post fractionation processes. This study demonstrates the possibility of using He-Ne-Ar content in natural gases to track gas evolution caused by recent basin activities.

Acknowledgements

The research was funded by SUERC and University of Glasgow. We are grateful to the Lan Yan Coalbed Methane Company for permission to collect samples and providing relevant information. The efforts of Dr Marta Zurakowska and Mr Terry Donnelly are appreciated for their assistance in the laboratories. We also thank Dr Anne Battani and Dr Magali Pujol for instructive discussions.

References

Al-Jubori, A., Johnston, S., Boyer, C., Lambert, S.W., Bustos, O.A., Pashin, J.C., Wray, A., 2009. Coalbed methane: clean energy for the world. Oilfield Rev., 21(2): 4-13.

Aravena, R., Harrison, S.M., Barker, J.F., Abercrombie, H., Rudolph, D., 2003. Origin of methane in the Elk Valley coalfield, southeastern British Columbia, Canada. Chem. Geol., 195(1–4): 219-227.

Bacsik, Z., Lopes, J.N.C., Gomes, M.F.C., Jancsó, G., Mink, J., Pádua, A.A.H., 2002. Solubility isotope effects in aqueous solutions of methane. J. Chem. Phys., 116(24): 10816-10824.

Bae, J.-S., Bhatia, S.K., 2006. High-pressure adsorption of methane and carbon dioxide on coal. Energy Fuels, 20(6): 2599-2607.

Ballentine, C.J., Burgess, R., Marty, B., 2002. Tracing Fluid Origin, Transport and Interaction in the Crust. In: Porcelli, D., Ballentine, C.J., Wieler, R. (Eds.), Rev. Mineral. Geochem., pp. 539-614.

Ballentine, C.J., Burnard, P.G., 2002. Production, Release and Transport of Noble Gases in the Continental Crust. In: Porcelli, D., Ballentine, C.J., Wieler, R. (Eds.), Rev. Mineral. Geochem., pp. 481-538.

Ballentine, C.J., Mazurek, M., Gautschi, A., 1994. Thermal constraints on crustal rare gas release and migration: Evidence from Alpine fluid inclusions. Geochim. Cosmochim. Acta, 58(20): 4333-4348.

Ballentine, C.J., O'Nions, R.K., 1992. The nature of mantle neon contributions to Vienna Basin hydrocarbon reservoirs. Earth Planet. Sci. Lett., 113(4): 553-567.

Ballentine, C.J., O'Nions, R.K., Oxburgh, E.R., Horvath, F., Deak, J., 1991. Rare gas constraints on hydrocarbon accumulation, crustal degassing and groundwater flow in the Pannonian Basin. Earth Planet. Sci. Lett., 105(1): 229-246.

Barry, P.H., Kulongoski, J.T., Landon, M.K., Tyne, R.L., Gillespie, J.M., Stephens, M.J., Hillegonds, D.J., Byrne, D.J., Ballentine, C.J., 2018. Tracing enhanced oil recovery signatures in casing gases from the Lost Hills oil field using noble gases. Earth Planet. Sci. Lett., 496: 57-67.

Barry, P.H., Lawson, M., Meurer, W.P., Warr, O., Mabry, J.C., Byrne, D.J., Ballentine, C.J., 2016. Noble gases solubility models of hydrocarbon charge mechanism in the Sleipner Vest gas field. Geochim. Cosmochim. Acta, 194: 291-309.

Battani, A., Sarda, P., Prinzhofer, A., 2000. Basin scale natural gas source, migration and trapping traced by noble gases and major elements: the Pakistan Indus basin. Earth Planet. Sci. Lett., 181(1): 229-249.

Bernard, B.B., Brooks, J.M., Sackett, W.M., 1976. Natural gas seepage in the Gulf of Mexico. Earth Planet. Sci. Lett., 31(1): 48-54.

Burruss, R.C., Laughrey, C.D., 2010. Carbon and hydrogen isotopic reversals in deep basin gas: Evidence for limits to the stability of hydrocarbons. Org. Geochem., 41(12): 1285-1296.

Byrne, D.J., Barry, P.H., Lawson, M., Ballentine, C.J., 2018. Determining gas expulsion vs retention during hydrocarbon generation in the Eagle Ford Shale using noble gases. Geochim. Cosmochim. Acta, 241: 240-254.

Cai, Y., Liu, D., Yao, Y., Li, J., Qiu, Y., 2011. Geological controls on prediction of coalbed methane of No. 3 coal seam in Southern Qinshui Basin, North China. Int. J. Coal Geol., 88(2–3): 101-112.

Cao, X., Li, S., Xu, L., Guo, L., Liu, L., Zhao, S., Liu, X., Dai, L., 2015. Mesozoic–Cenozoic evolution and mechanism of tectonic geomorphology in the central North China Block: Constraint from apatite fission track thermochronology. J. Asian Earth Sci., 114: 41-53.

Castro, M.C., Jambon, A., Marsily, G., Schlosser, P., 1998. Noble gases as natural tracers of water circulation in the Paris Basin: 1. Measurements and discussion of their origin and mechanisms of vertical transport in the basin. Water Resour. Res., 34(10): 2443-2466.

Chen, Z., Song, Y., Qin, S., 2007. Geochemical characteristics of CBM reservoirs in southern Qinshui Basin. Nat. Gas Geosci., 18: 561-564. (in Chinese with English abstract)

Clayton, C., 1991. Carbon isotope fractionation during natural gas generation from kerogen. Mar. Petroleum Geol., 8(2): 232-240.

509 Craig, H., 1957. Isotopic standards for carbon and oxygen and correction factors for mass-
510 spectrometric analysis of carbon dioxide. Geochim. Cosmochim. Acta, 12(1): 133-149.
511 Craig, H., Lupton, J.E., 1976. Primordial neon, helium, and hydrogen in oceanic basalts. Earth Planet.
512 Sci. Lett., 31(3): 369-385.
513 Crovetto, R., Fernández-Prini, R., Japas, M.L., 1982. Solubilities of inert gases and methane in H_2O
514 and in D_2O in the temperature range of 300 to 600 K. J. Chem. Phys., 76(2): 1077-1086.
515 Donnelly, T., Waldron, S., Tait, A., Dougans, J., Bearhop, S., 2001. Hydrogen isotope analysis of
516 natural abundance and deuterium-enriched waters by reduction over chromium on-line to a
517 dynamic dual inlet isotope-ratio mass spectrometer. Rapid Commun. Mass Spectrom., 15(15):
518 1297-1303.
519 Dunbar, E., Cook, G.T., Naysmith, P., Tripney, B.G., Xu, S., 2016. AMS ^{14}C Dating at the Scottish
520 Universities Environmental Research Centre (SUERC) Radiocarbon Dating Laboratory.
521 Radiocarbon, 58(01): 9-23.
522 Eberhardt, P., Eugster, O., Marti, K., 1965. Notizen: A Redetermination of the Isotopic Composition
523 of Atmospheric Neon, Z. Naturforsch., 623-624.
524 Flores, R.M., 1998. Coalbed methane: From hazard to resource. Int. J. Coal Geol., 35(1–4): 3-26.
525 Flores, R.M., Rice, C.A., Stricker, G.D., Warden, A., Ellis, M.S., 2008. Methanogenic pathways of
526 coal-bed gas in the Powder River Basin, United States: The geologic factor. Int. J. Coal Geol.,
527 76(1–2): 52-75.
528 Gautheron, C., Moreira, M., 2002. Helium signature of the subcontinental lithospheric mantle. Earth
529 Planet. Sci. Lett., 199(1): 39-47.
530 Golding, S.D., Boreham, C.J., Esterle, J.S., 2013. Stable isotope geochemistry of coal bed and shale
531 gas and related production waters: A review. Int. J. Coal Geol., 120: 24-40.
532 Gonfiantini, R., 1978. Standards for stable isotope measurements in natural compounds. Nature, 271:
533 534.
534 Györe, D., Tait, A., Hamilton, D., Stuart, F.M. The formation of NeH^+ in static vacuum mass
535 spectrometers and re-determination of $^{21}Ne/^{20}Ne$ of air. Geochim. Cosmochim. Acta 263, 1-
536 12.
537 Györe, D., McKavney, R., Gilfillan, S.M.V., Stuart, F.M., 2018. Fingerprinting coal-derived gases
538 from the UK. Chem. Geol., 480: 75-85.
539 Györe, D., Stuart, F.M., Gilfillan, S.M.V., Waldron, S., 2015. Tracing injected CO_2 in the Cranfield
540 enhanced oil recovery field (MS, USA) using He, Ne and Ar isotopes. Int. J. Greenh. Gas
541 Cont., 42: 554-561.
542 Han, F., Busch, A., Krooss, B.M., Liu, Z., van Wageningen, N., Yang, J., 2010a. Experimental study
543 on fluid transport processes in the cleat and matrix systems of coal. Energy Fuels, 24(12):
544 6653-6661.
545 Han, F., Busch, A., van Wageningen, N., Yang, J., Liu, Z., Krooss, B.M., 2010b. Experimental study
546 of gas and water transport processes in the inter-cleat (matrix) system of coal: Anthracite
547 from Qinshui Basin, China. Int. J. Coal Geol., 81(2): 128-138.
548 Hildenbrand, A., Ghanizadeh, A., Krooss, B.M., 2012. Transport properties of unconventional gas
549 systems. Mar. Petroleum Geol., 31(1): 90-99.
550 Hoşgörmez, H., Namık Yalçın, M., Cramer, B., Gerling, P., Faber, E., Schaefer, R.G., Mann, U.,
551 2002. Isotopic and molecular composition of coal-bed gas in the Amasra region (Zonguldak
552 basin—western Black Sea). Org. Geochem., 33(12): 1429-1439.
553 Hu, G., Liu, S., Li, J., Zhang, L., Li, Z., 2001. Origin of coal-bed gases in Jincheng area of Qinshui
554 Basin. Oil and Gas Geol., 22: 319-321. (in Chinese with English abstract)
555 Kaneoka, I., 1980. Rare gas isotopes and mass fractionation: An indicator of gas transport into or
556 from a magma. Earth Planet. Sci. Lett., 48(2): 284-292.
557 Kinnon, E.C.P., Golding, S.D., Boreham, C.J., Baublys, K.A., Esterle, J.S., 2010. Stable isotope and
558 water quality analysis of coal bed methane production waters and gases from the Bowen
559 Basin, Australia. Int. J. Coal Geol., 82(3–4): 219-231.
560 Kipfer, R., Aeschbach-Hertig, W., Peeters, F., Stute, M., 2002. Noble gases in lakes and ground
561 waters. In: Porcelli, D., Ballentine, C.J., Wieler, R. (Eds.), Rev. Mineral. Geochem., pp. 615-
562 700.

Kotarba, M.J., Rice, D.D., 2001. Composition and origin of coalbed gases in the Lower Silesian basin, southwest Poland. Appl. Geochem., 16(7–8): 895-910.
Laxminarayana, C., Crosdale, P.J., 1999. Role of coal type and rank on methane sorption characteristics of Bowen Basin, Australia coals. Int. J. Coal Geol., 40(4): 309-325.
Lee, J.-Y., Marti, K., Severinghaus, J.P., Kawamura, K., Yoo, H.-S., Lee, J.B., Kim, J.S., 2006. A redetermination of the isotopic abundances of atmospheric Ar. Geochim. Cosmochim. Acta, 70(17): 4507-4512.
Li, J., Bai, P., Mao, H., Han, W., Wang, X., Zhang, J., 2014. Analysis of geochemistry characteristics and its origin of CBM in Zhengzhuang and Hudi blocks. J. China Coal Soc., 39(9): 1802-1811. (in Chinese with English abstract)
Ma, X., Song, Y., Liu, S., Jiang, L., Hong, F., 2016. Experimental study on history of methane adsorption capacity of Carboniferous-Permian coal in Ordos Basin, China. Fuel, 184: 10-17.
Mark, D.F., Stuart, F.M., de Podesta, M., 2011. New high-precision measurements of the isotopic composition of atmospheric argon. Geochim. Cosmochim. Acta, 75(23): 7494-7501.
Matsuda, J., Matsumoto, T., Sumino, H., Nagao, K., Yamamoto, J., Miura, Y., Kaneoka, I., Takahata, N., Sano, Y., 2002. The $^{3}He/^{4}He$ ratio of the new internal He Standard of Japan (HESJ). Geochem. J., 36(2): 191-195.
Meng, Z., Zhang, J., Wang, R., 2011. In-situ stress, pore pressure and stress-dependent permeability in the Southern Qinshui Basin. Int. J. Rock Mech. Min. Sci., 48(1): 122-131.
Mishima, K., Sumino, H., Yamada, T., Ieki, S., Nagakura, N., Otono, H., Oide, H., 2018. Accurate determination of the absolute $^{3}He/^{4}He$ ratio of a synthesized helium standard gas (helium standard of Japan, HESJ): Toward revision of the atmospheric $^{3}He/^{4}He$ ratio. Geochem. Geophys., 19(10): 3995-4005.
Moore, M.T., Vinson, D.S., Whyte, C.J., Eymold, W.K., Walsh, T.B., Darrah, T.H., 2018. Differentiating between biogenic and thermogenic sources of natural gas in coalbed methane reservoirs from the Illinois Basin using noble gas and hydrocarbon geochemistry. Geol. Soc. London, Spec. Publ., 468.
Moore, T.A., 2012. Coalbed methane: A review. Int. J. Coal Geol., 101: 36-81.
Morrison, P., Pine, J., 1954. Radiogenic origin of the helium isotopes in rock. Trans. N. Y. Acad. Sci., 16 (3 Series II): 146-147.
Ozima, M., Podosek, F.A., 2002. Noble gas geochemistry (2nd Ed.). Cambridge University Press, Cambridge.
Peeters, F., Beyerle, U., Aeschbach-Hertig, W., Holocher, J., Brennwald, M.S., Kipfer, R., 2003. Improving noble gas based paleoclimate reconstruction and groundwater dating using $^{20}Ne/^{22}Ne$ ratios. Geochim. Cosmochim. Acta, 67(4): 587-600.
Qin, S., Tang, X., Song, Y., Wang, H., 2006. Distribution and fractionation mechanism of stable carbon isotope of coalbed methane. Sci. China Ser. D-Earth Sci., 49(12): 1252-1258.
Ren, Z., Xiao, H., Liu, L., Zhang, S., Qin, Y., Wei, C., 2005. The evidence of fission-track data for the study of tectonic thermal history in Qinshui Basin. Chin. Sci. Bull., 50: 104-110.
Rice, D.D., 1993. Composition and origins of coalbed gas. AAPG Stud. Geol., 38(1): 159-184.
Schoell, M., 1980. The hydrogen and carbon isotopic composition of methane from natural gases of various origins. Geochim. Cosmochim. Acta, 44(5): 649-661.
Sherwood Lollar, B., Ballentine, C.J., Onions, R.K., 1997. The fate of mantle-derived carbon in a continental sedimentary basin: Integration of C/He relationships and stable isotope signatures. Geochim. Cosmochim. Acta, 61(11): 2295-2307.
Shimizu, S., Akiyama, M., Naganuma, T., Fujioka, M., Nako, M., Ishijima, Y., 2007. Molecular characterization of microbial communities in deep coal seam groundwater of northern Japan. Geobiol., 5(4): 423-433.
Smith, S.P., Kennedy, B.M., 1983. The solubility of noble gases in water and in NaCl brine. Geochim. Cosmochim. Acta, 47(3): 503-515.
Song, Y., Liu, S., Zhang, Q., Tao, M., Zhao, M., Hong, F., 2012. Coalbed methane genesis, occurrence and accumulation in China. Petroleum Sci., 9(3): 269-280.
Song, Y., Ma, X., Liu, S., Jiang, L., Hong, F., Qin, Y., 2018. Accumulation conditions and key technologies for exploration and development of Qinshui coalbed methane field. Petroleum Res., 3(4): 320-335.

618 Strąpoć, D., Mastalerz, M., Dawson, K., Macalady, J., Callaghan, A.V., Wawrik, B., Turich, C.,
619 Ashby, M., 2011. Biogeochemistry of microbial coal-bed methane. Annu. Rev. Earth Planet.
620 Sci., 39(1): 617-656.
621 Strąpoć, D., Mastalerz, M., Eble, C., Schimmelmann, A., 2007. Characterization of the origin of
622 coalbed gases in southeastern Illinois Basin by compound-specific carbon and hydrogen
623 stable isotope ratios. Org. Geochem., 38(2): 267-287.
624 Su, X., Lin, X., Liu, S., Zhao, M., Song, Y., 2005. Geology of coalbed methane reservoirs in the
625 Southeast Qinshui Basin of China. Int. J. Coal Geol., 62(4): 197-210.
626 Tao, M., Shi, B., Li, J., Wang, W., Li, X., Gao, B., 2007. Secondary biological coalbed gas in the
627 Xinji area, Anhui province, China: Evidence from the geochemical features and secondary
628 changes. Int. J. Coal Geol., 71(2–3): 358-370.
629 Torgersen, T., 1980. Controls on pore-fluid concentration of ^{4}He and ^{222}Rn and the calculation of
630 $^{4}He/^{222}Rn$ ages. J. Geochem. Explor., 13(1): 57-75.
631 Torgersen, T., Kennedy, B.M., 1999. Air-Xe enrichments in Elk Hills oil field gases: role of water in
632 migration and storage. Earth Planet. Sci. Lett., 167(3–4): 239-253.
633 Torgersen, T., Kennedy, B.M., Hiyagon, H., Chiou, K.Y., Reynolds, J.H., Clarke, W.B., 1989. Argon
634 accumulation and the crustal degassing flux of ^{40}Ar in the Great Artesian Basin, Australia.
635 Earth Planet. Sci. Lett., 92(1): 43-56.
636 USEIA, 2013. Annual energy outlook 2013, US Energy Information Administration, Washington,
637 DC.
638 Wang, B., Sun, F., Tang, D., Zhao, Y., Song, Z., Tao, Y., 2015. Hydrological control rule on coalbed
639 methane enrichment and high yield in FZ Block of Qinshui Basin. Fuel, 140: 568-577.
640 Wang, H., Fu, X., Zhang, X., Niu, Q., Ge, Y., Tian, J., Cheng, X., Chen, N., Hou, X., Du, H., 2018.
641 Source, age, and evolution of coal measures water in central-south Qinshui Basin, China.
642 Energy Fuels, 32(7): 7358-7373.
643 Wang, Y., Zhang, Q., Zhu, W., Wang, L., Xie, G., Ge, R., Liu, C., Zou, X., 2014. Meso-cenozoic
644 structural deformation and tectonic stress fields in the south margin of Qinshui Basin. Geol. J.
645 China Univ., 20(2): 249-259. (in Chinese with English abstract)
646 Wang, Z., Tang, S., Sun, P., Zheng, G., 2013. Feasibility study of multi-layer drainage for No. 3 and 9
647 coal seams in Shouyang Block, Qinshui Basin. Coal Geol. China, 25(11): 21-26. (in Chinese
648 with English abstract)
649 Whiticar, M.J., 1996. Stable isotope geochemistry of coals, humic kerogens and related natural gases.
650 Int. J. Coal Geol., 32(1): 191-215.
651 Xia, X., Tang, Y., 2012. Isotope fractionation of methane during natural gas flow with coupled
652 diffusion and adsorption/desorption. Geochim. Cosmochim. Acta, 77: 489-503.
653 Xu, S., Nakai, S.i., Wakita, H., Wang, X., 1995. Mantle-derived noble gases in natural gases from
654 Songliao Basin, China. Geochim. Cosmochim. Acta, 59(22): 4675-4683.
655 Xu, W., Wang, D., Wang, Q., Pei, F., Lin, J., 2004. $^{40}Ar/^{39}Ar$ dating of hornblende and biotite in
656 Mesozoic intrusive complex from the North China Block: Constraints on the time of
657 lithospheric thining. Geochimica, 33(3): 221-231. (in Chinese with English abstract)
658 Yatsevich, I., Honda, M., 1997. Production of nucleogenic neon in the Earth from natural radioactive
659 decay. J. Geophys. Res.: Solid Earth, 102(B5): 10291-10298.
660 Yin, S., Ding, W., Hu, Q., Liu, J., Mei, Y., Liu, Z., 2016. Hydrocarbon source rock characteristics and
661 favorable hydrocarbon-generating area evaluation of Carboniferous-Permian coal measures
662 strata in Qinshui basin, Shanxi, China. J. Chengdu Univ. Technol. (Sci. & Technol. Ed.),
663 43(2): 163-176. (in Chinese with English abstract)
664 Zartman, R., Wasserburg, G., Reynolds, J., 1961. Helium, argon, and carbon in some natural gases. J.
665 Geophys. Res., 66(1): 277-306.
666 Zazzeri, G., Lowry, D., Fisher, R.E., France, J.L., Lanoisellé, M., Kelly, B.F.J., Necki, J.M., Iverach,
667 C.P., Ginty, E., Zimnoch, M., Jasek, A., Nisbet, E.G., 2016. Carbon isotopic signature of
668 coal-derived methane emissions to the atmosphere: from coalification to alteration. Atmos.
669 Chem. Phys., 16(21): 13669-13680.
670 Zeng, Y., Fan, B., Liu, H., Wang, C., 1999. A analysis to the history of thermal evolution
671 hydrocarbon- generating and the heat source about main seam of Shanxi formation in

672 southeastern Shanxi Province. Sci. Geol. Sinica, 34(1): 90-98. (in Chinese with English
673 abstract)
674 Zhang, E., Hill, R.J., Katz, B.J., Tang, Y., 2008. Modeling of gas generation from the Cameo coal
675 zone in the Piceance Basin, Colorado. AAPG Bulletin, 92(8): 1077-1106.
676 Zhang, J., Liu, D., Cai, Y., Yao, Y., Ge, X., 2018. Carbon isotopic characteristics of CH_4 and its
677 significance to the gasperformance of coal reservoirs in the Zhengzhuang area, Southern
678 Qinshui Basin, North China. J. Nat. Gas Sci. Eng., 58: 135-151.
679 Zhang, J., Tao, M., 2000. Geological significances of coal bed methane carbon isotope in coal bed
680 methane exploration. Acta Sedimentol. Sin., 18(4): 611-614. (in Chinese with English
681 abstract)
682 Zhang, J.Y., Zheng, C.G., Ren, D.Y., Chou, C.L., Liu, J., Zeng, R.S., Wang, Z.P., Zhao, F.H., Ge,
683 Y.T., 2004. Distribution of potentially hazardous trace elements in coals from Shanxi
684 province, China. Fuel, 83(1): 129-135.
685 Zhang, S., Tang, S., Li, Z., Guo, Q., Pan, Z., 2015. Stable isotope characteristics of CBM co-produced
686 water and implications for CBM development: The example of the Shizhuangnan block in the
687 southern Qinshui Basin, China. J. Nat. Gas Sci. Eng., 27, Part 3: 1400-1411.
688 Zhang, S., Zhang, X., Li, G., Liu, X., Zhang, P., 2019. Distribution characteristics and geochemistry
689 mechanisms of carbon isotope of coalbed methane in central-southern Qinshui basin, China.
690 Fuel, 244: 1-12.
691 Zhao, F., 1997. Study on the mechanism of distributions and occurrences of hazardous minor and
692 trace elements in coal and leaching experiments of coal combustion residues, PhD thesis,
693 China University of Mining & Technology. (in Chinese with English abstract)
694 Zhao, L., Ward, C.R., French, D., Graham, I.T., Dai, S., Yang, C., Xie, P., Zhang, S., 2018. Origin of
695 a kaolinite-NH_4-illite-pyrophyllite-chlorite assemblage in a marine-influenced anthracite and
696 associated strata from the Jincheng Coalfield, Qinshui Basin, Northern China. Int. J. Coal
697 Geol., 185: 61-78.
698 Zhou, Z., Ballentine, C.J., 2006. ^{4}He dating of groundwater associated with hydrocarbon reservoirs.
699 Chem. Geol., 226(3–4): 309-327.
700 Zhou, Z., Ballentine, C.J., Kipfer, R., Schoell, M., Thibodeaux, S., 2005. Noble gas tracing of
701 groundwater/coalbed methane interaction in the San Juan Basin, USA. Geochim. Cosmochim.
702 Acta, 69(23): 5413-5428.

703 **Figure 1**

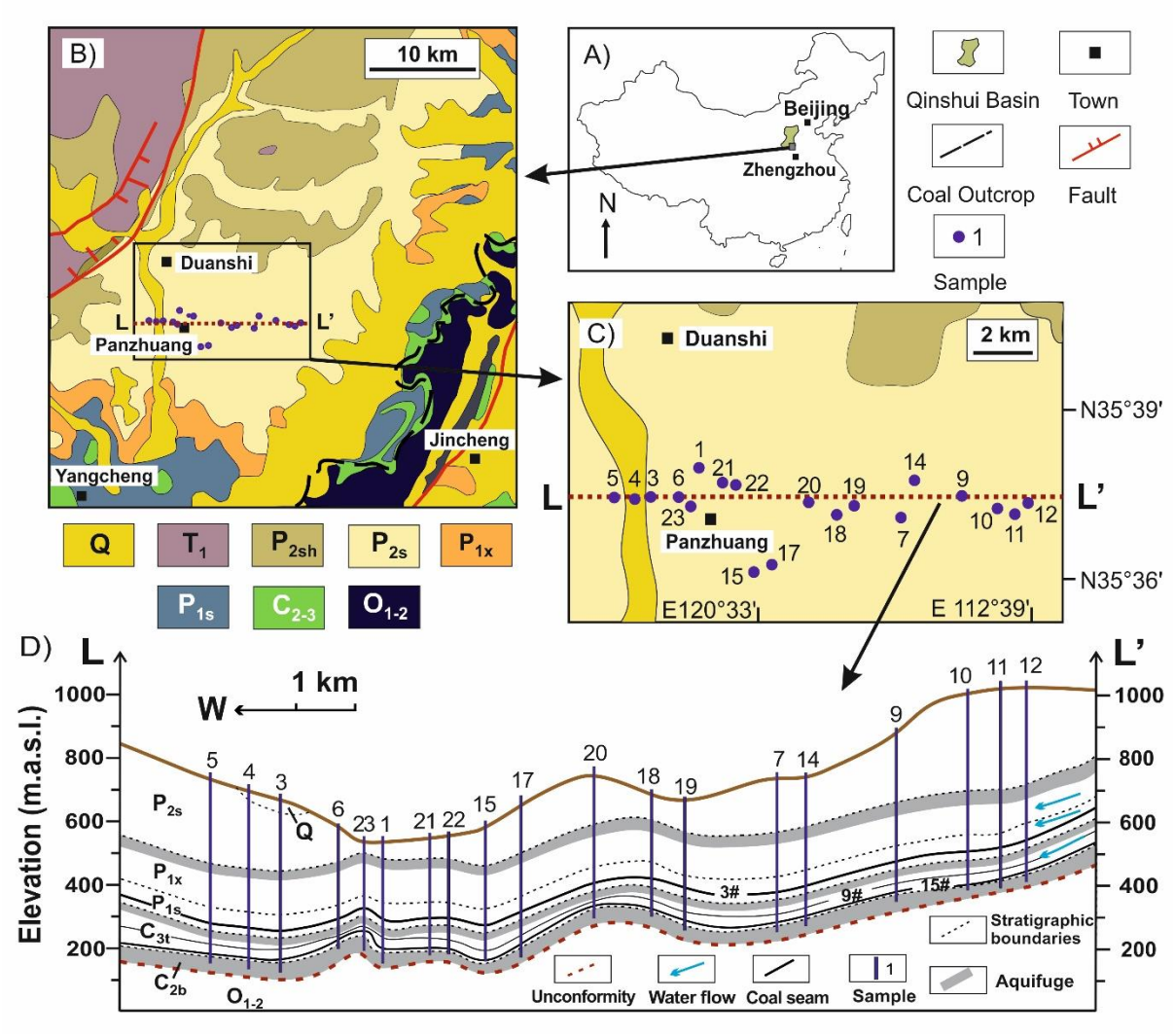

704

705 **Figure 2**

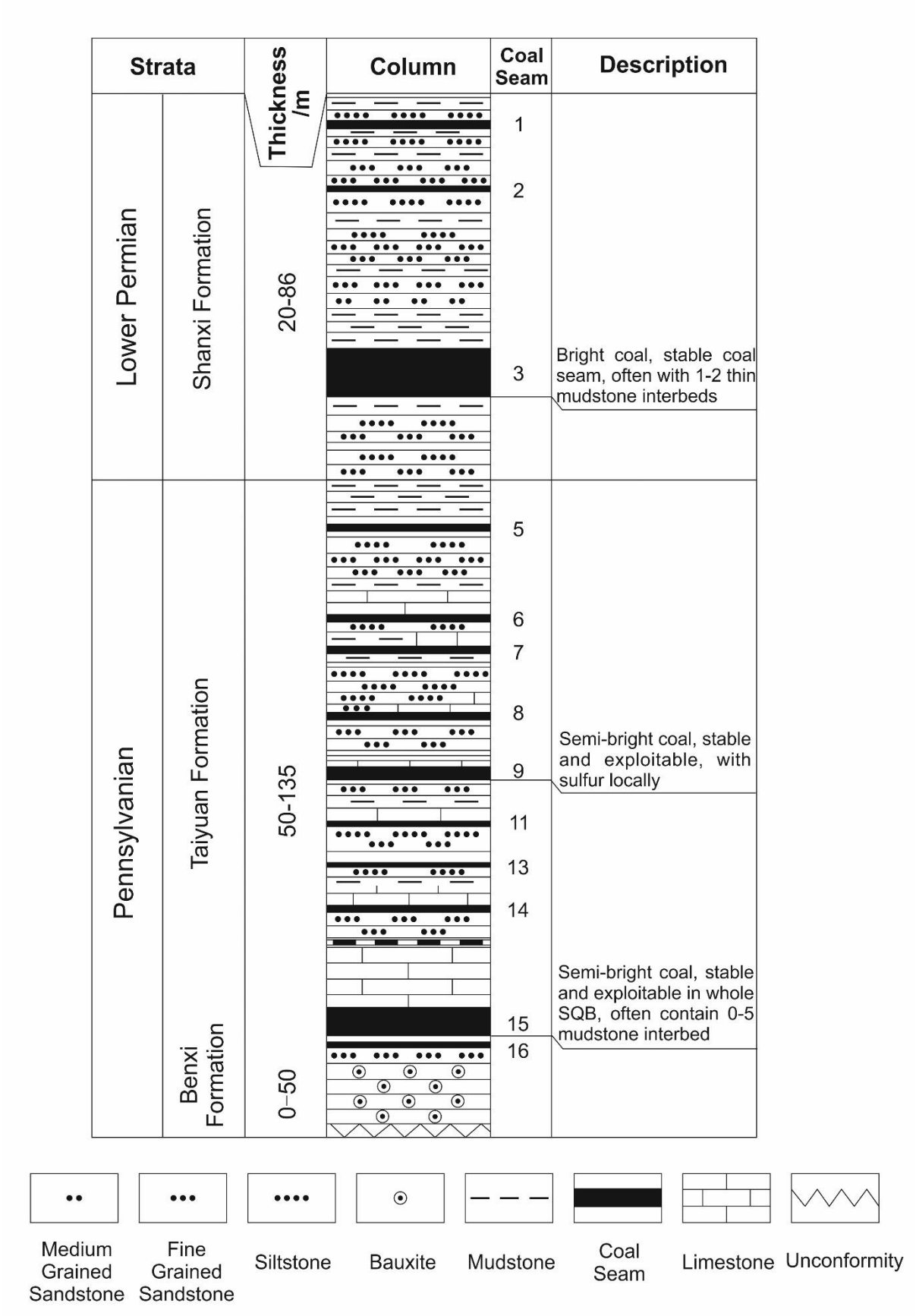

706

707 **Figure 3**

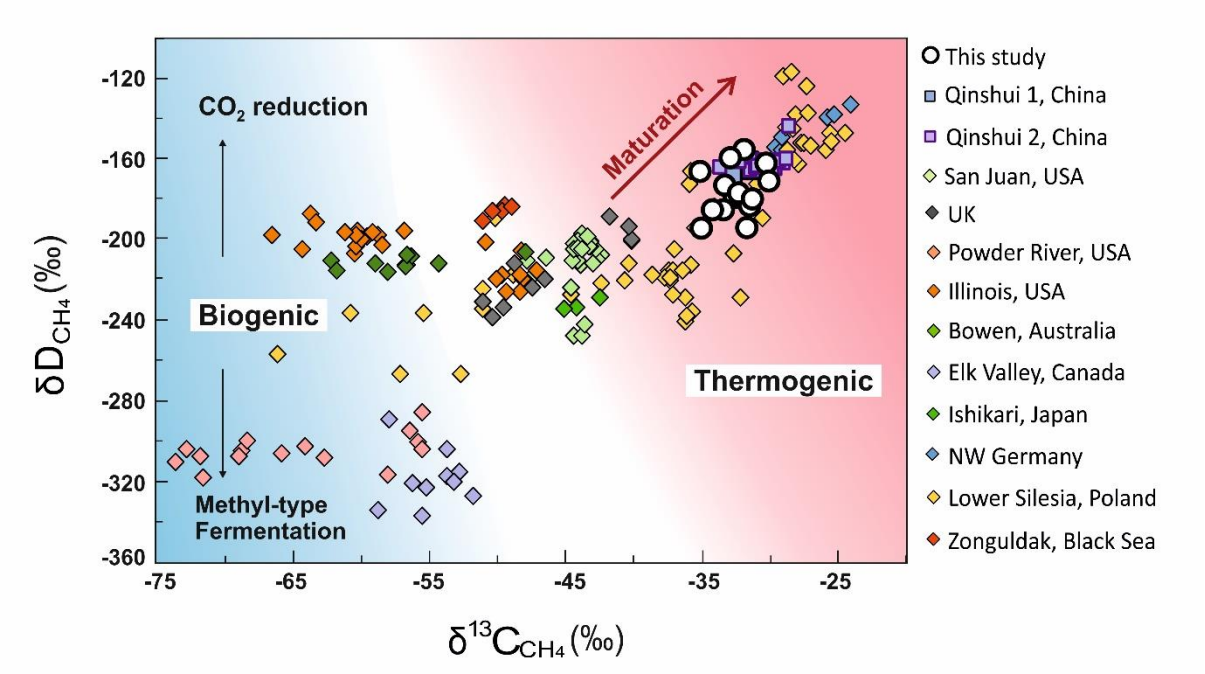

708

709 **Figure 4**

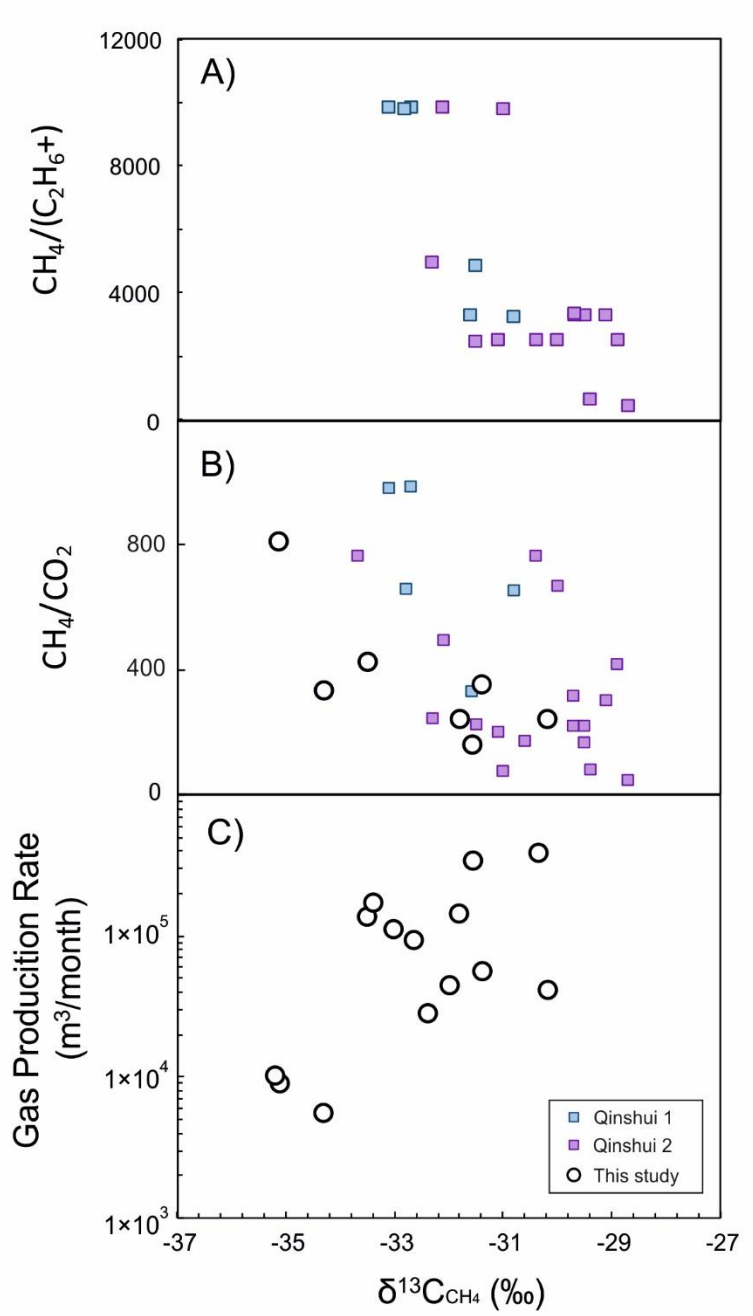

710

711 **Figure 5**

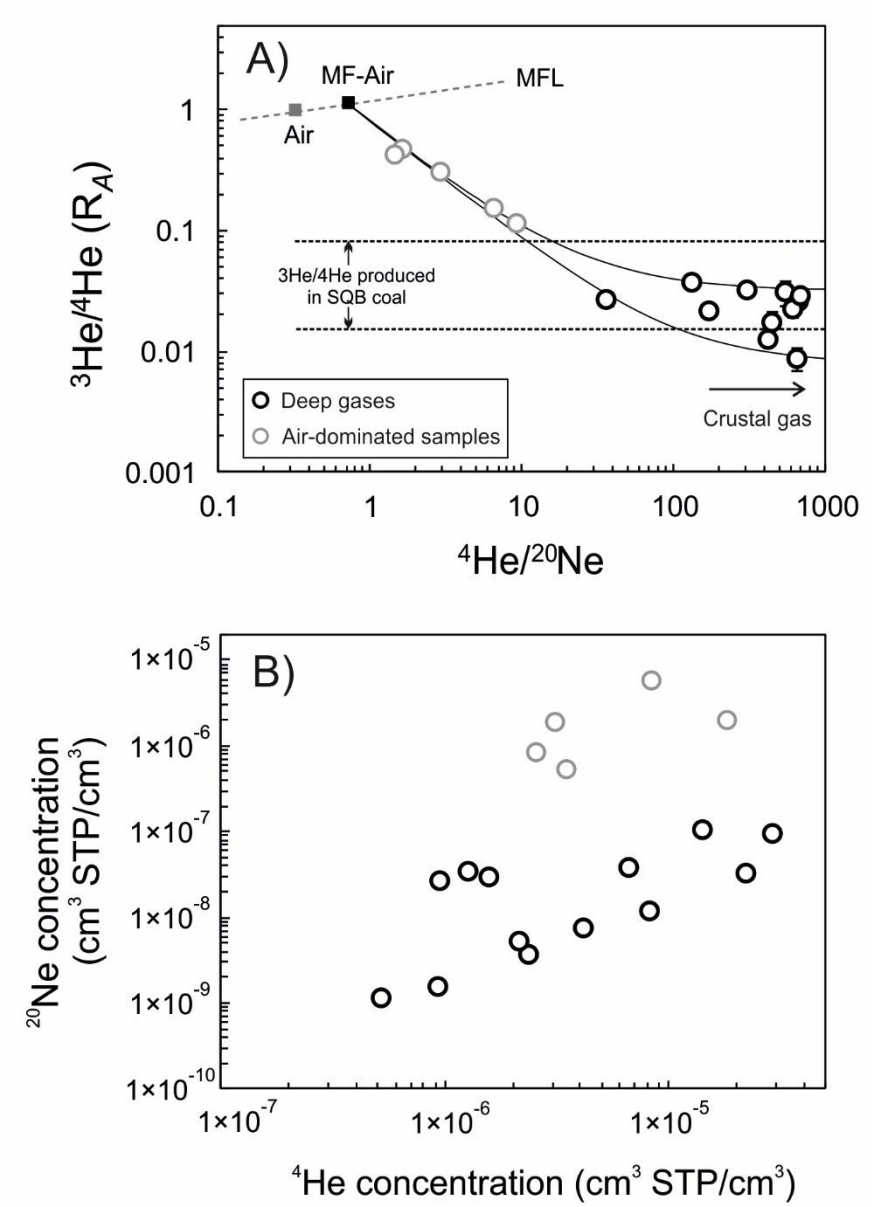

712

713 **Figure 6**

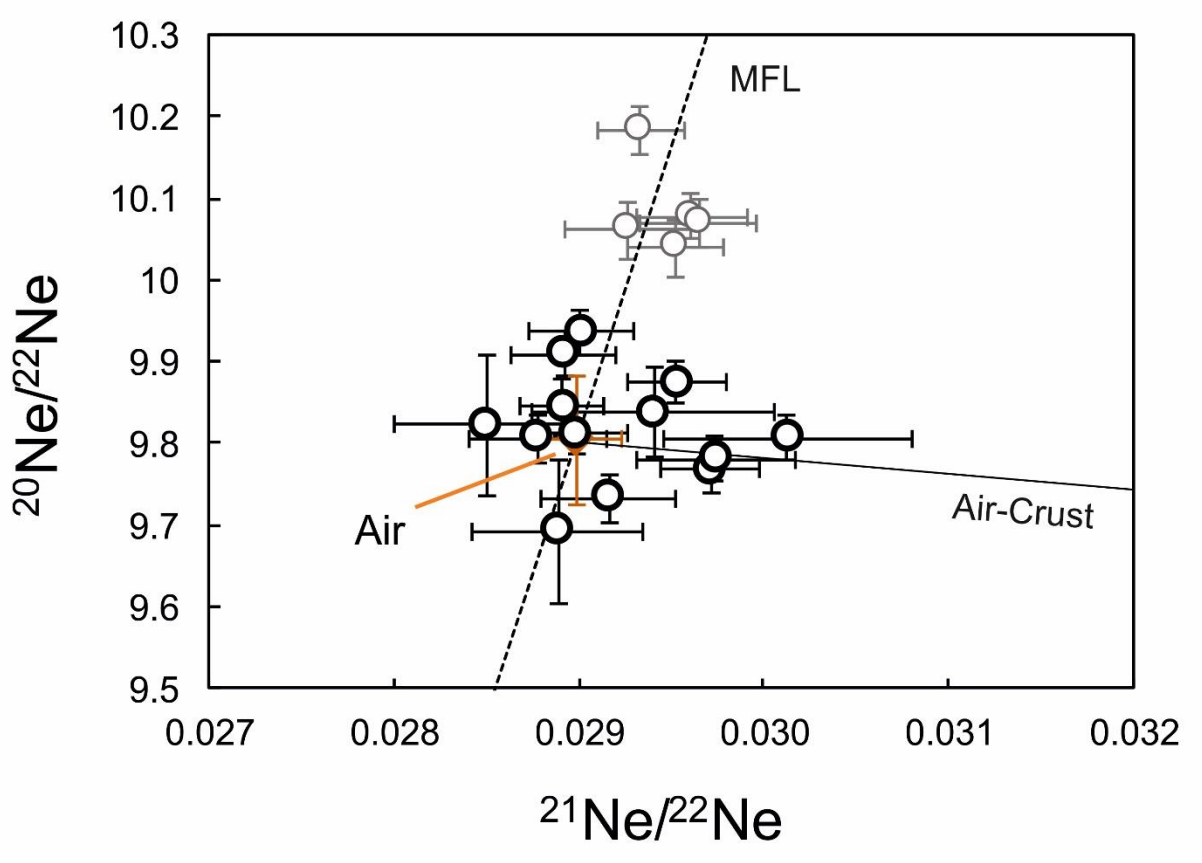

714

715 **Figure 7**

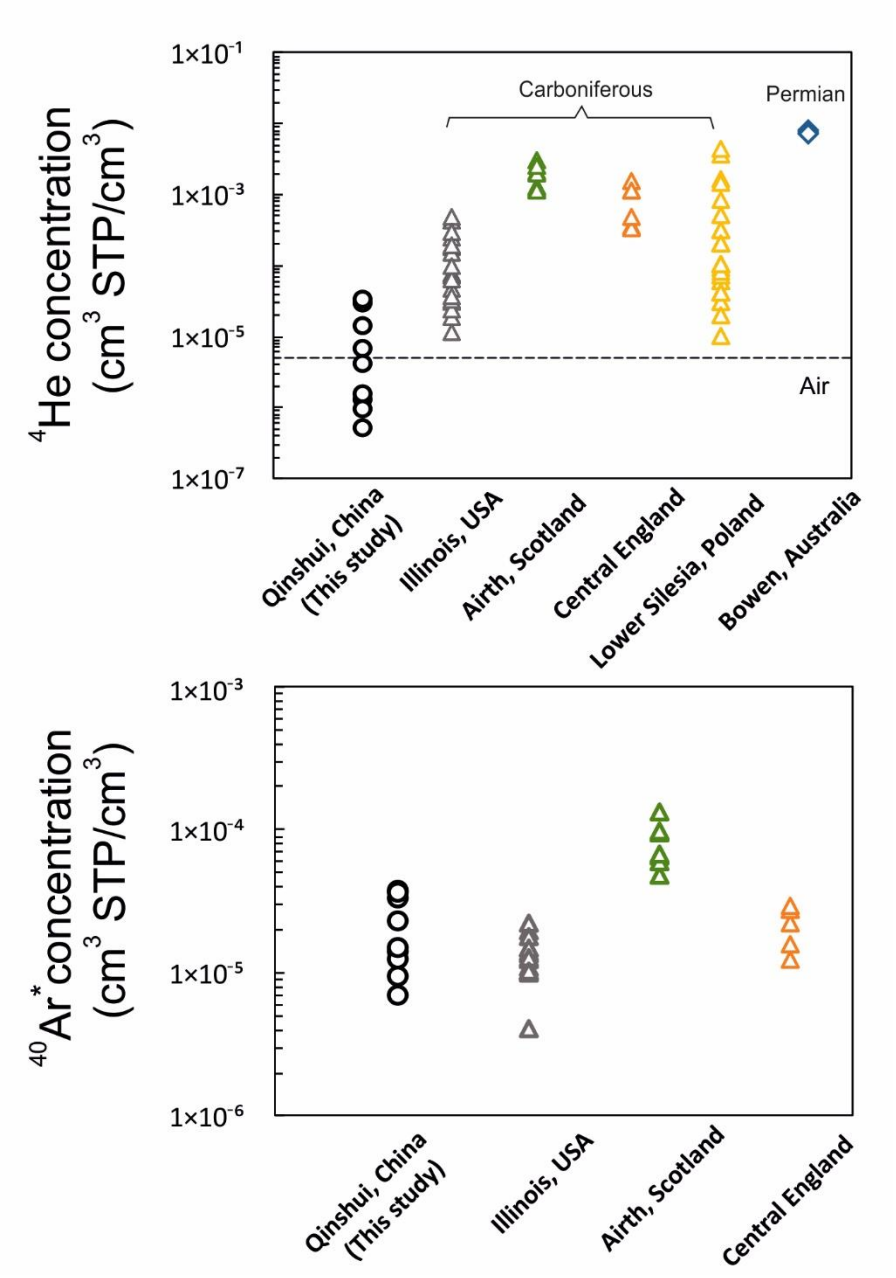

716

717 **Figure 8**

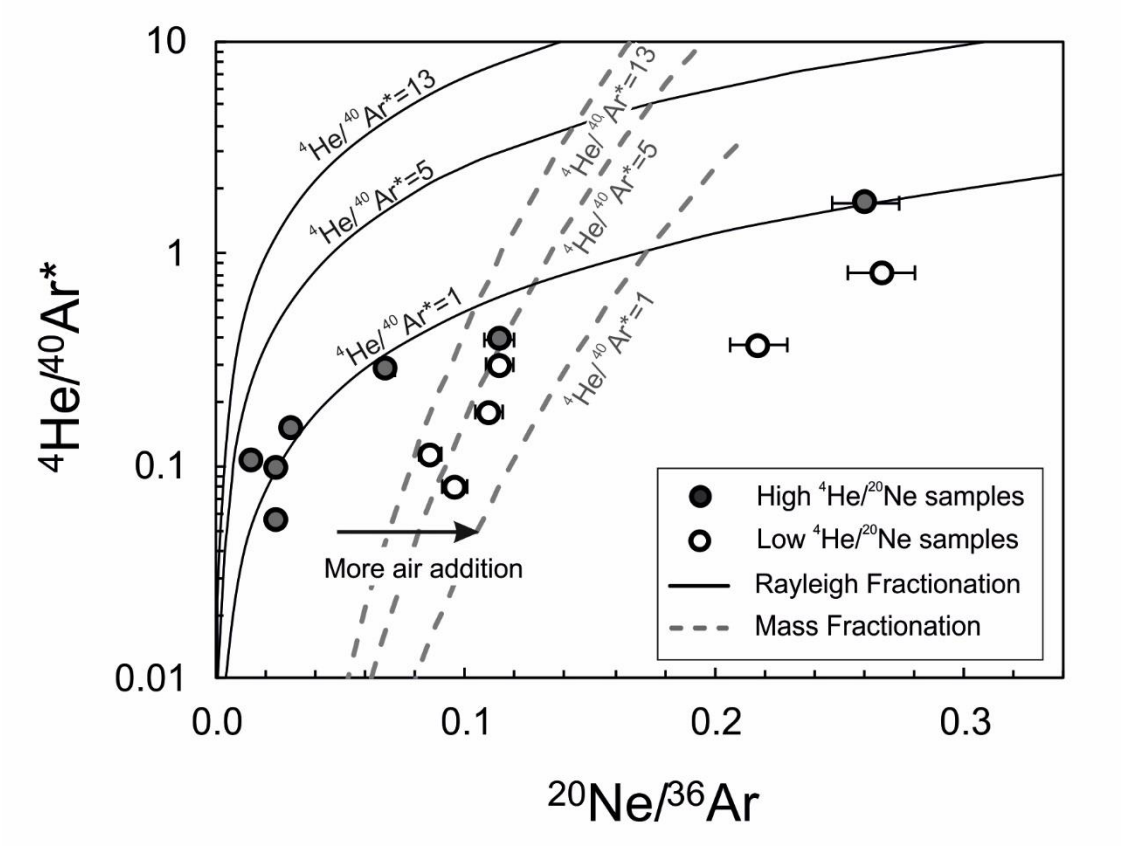

718

Figure Captions

Figure 1. Location and geologic map of the southeast Qinshui Basin (China). A) The location of study area in China; B) Simplified geological map of southeast Qinshui Basin; C) Location of wells sampled in this study; D) Simplified hydrological cross-section of the basin along the line L-L' above. Figures are modified after Wang et al. (2014) and Zhang et al. (2015).

Figure 2. Stratigraphic column of the coal-bearing formations in southeast Qinshui Basin. Modified after Su et al. (2005) and Cai et al. (2011).

Figure 3. Genetic characterization of methane from SQB. Data from this study show that methane is thermogenic in origin. Data sources: San Juan (Zhou et al., 2005); UK (Györe et al., 2018); Powder River (Flores et al., 2008); Illinois (Moore et al., 2018; Strąpoć et al., 2007); Bowen (Kinnon et al., 2010); Elk Valley (Aravena et al., 2003); Ishikari (Shimizu et al., 2007); NW Germany (Schoell, 1980); Lower Silesia (Kotarba and Rice, 2001); Black Sea (Hoşgörmez et al., 2002); Qinshui 1 (Li et al., 2014); Qinshui 2 (Zhang et al., 2018). 1 σ errors are covered by printed symbols. Modified after Strąpoć et al. (2011).

Figure 4. The relationship between $\delta^{13}C_{CH4}$ with molecular composition of gases and gas production rate. The evident negative trends between $\delta^{13}C_{CH4}$ and $CH_4/(C_2H_{6+})$ (A), CH_4/CO_2 (B) and positive trend between $\delta^{13}C$ and gas production rate (C) indicate that molecular and isotopic compositions of produced gases have been affected by the diffusive fractionation process during gas extraction. Data source: Qinshui 1 (Li et al., 2014); Qinshui 2 (Zhang et al., 2018). 1 σ errors are covered by printed symbols.

Figure 5. The He and Ne systematics of CBM gases from SQB. A) $^3He/^4He$ ratio plotted against $^4He/^{20}Ne$ of SQB methane. The solid black lines are mixing lines between deep gases, with high $^4He/^{20}Ne$, and mass fractionated air. The range of $^3He/^4He$ of radiogenic He produced within the coals (see text) is shown by black dashed lines. MFL: Mass fractionation line after square root law(Kaneoka, 1980). The black circles represent deep gases; grey circles represent air-dominated samples. The black and grey squares represent the mass fractionated air and air, respectively. B) ^{20}Ne vs. ^4He concentrations. Air-dominated samples have relatively higher ^{20}Ne concentration but similar ^4He concentration range with deep gases. Uncertainties are 1 σ.

748 **Figure 6.** $^{20}Ne/^{22}Ne$ vs. $^{21}Ne/^{22}Ne$ for SQB methane-rich gases. Air is after Eberhardt et al.
749 (1965) and Györe et al. (2019). The air-dominated samples (grey circles) are following the
750 mass-controlled fractionation line (MFL) in consistent with He-Ne molecular trend. The deep
751 gases (black circles) are mainly air-derived without evident crustal addition of ^{21}Ne.
752 Uncertainties are 1 σ.

753 **Figure 7.** He and Ar contents of Carboniferous and Permian coals worldwide. The
754 concentration of ^{4}He in the SQB is evidently lower than that in other basins with similar age
755 (A). $^{40}Ar^{*}$ concentrations in gases from SQB overlaps with that in other basins (B). Data
756 source: Illinois, USA (Moore et al., 2018); Airth, Scotland (Györe et al., 2018); Central
757 England (Györe et al., 2018); Lower Silesia, Poland (Kotarba and Rice, 2001), Bowen,
758 Australia (Kinnon et al., 2010). 1 σ errors are covered by printed symbols.

759 **Figure 8.** $^{4}He/^{40}Ar^{*}$ vs. $^{20}Ne/^{36}Ar$ for Southeast Qinshui Basin CBM. The black lines reflect
760 solubility-controlled Rayleigh fractionation of open system with an initial $^{20}Ne/^{36}Ar$ of 0.154.
761 The grey dashed lines are mass-controlled kinetic fractionation (Ballentine et al., 2002; Zhou
762 et al., 2005). Open system Rayleigh fractionation of gas from formation water with initial
763 $^{4}He/^{40}Ar^{*} = 1$ provides the best fit to the least air-contaminated gas samples (black filled
764 circles, $^{4}He/^{20}Ne$ >400). This implies that radiogenic ^{4}He and ^{40}Ar in the reservoir were
765 dissolved in the formation water and degassed with air-derived ^{20}Ne and ^{36}Ar during pumping
766 process.

Tables

Table 1. Gas compositions and stable isotopes of coalbed methane from southeast Qinshui Basin.

Sample ID	Depth (m)	Distance to the basin margin (km)	Gas extraction duration (month)	Total gas production ($\times 10^5$)	CH_4/CO_2	$\delta^{13}C$	δD
Qs1	406	20.2	132	125	na	-32.7	-178
Qs3	567	21.3	86	24.4	na	-32.4	-176
Qs4	585	21.8	25	41	na	na	na
Qs5	606	22.5	96	335	152	-31.6	-183
Qs6	390	20.4	96	377	na	-30.4	-162
Qs7	529	13.8	83	105	na	na	na
Qs9	552	12.0	69	39.1	349	-31.4	-180
Qs10	638	10.8	99	138	423	-33.5	-185
Qs11	673	10.2	125	217	na	-33.4	-173
Qs12	660	9.9	128	57.9	na	-32.0	-155
Qs14	487	13.6	71	6.51	806	-35.1	-194
Qs15	446	17.4	23	10.4	na	na	na
Qs17	519	16.8	15	0.85	329	-34.3	-185
Qs18	394	15.3	24	2.5	na	-35.2	-166
Qs19	420	14.9	3	0.29	na	na	na
Qs20	482	16.5	27	52.7	330	na	na
Qs21	375	19.3	25	36.7	237	-31.8	-194
Qs22	390	18.9	26	29.1	na	-33.0	-159
Qs23	361	20.0	96	40.5	235	-30.2	-171

1σ standard deviation for C_1/C_{2+}, CH_4/CO_2, $\delta^{13}C$ and δD are 2%, 2%, 0.3‰ and 3‰, respectively.

δC_{CH4} and δD_{CH4} are in permil and relative to PDB (Craig, 1957) and V-SMOW (Gonfiantini, 1978), respectively.

Volume of produced gas is given in m^3 STP, where standard conditions are: p=0.101 MPa and T=0 °C.

na: not analysed.

774 Table 2. Noble gas compositions of well gases from southeast Qinshui Basin.

Sample ID	^{4}He ($\times10^{-6}$)	^{20}Ne ($\times10^{-8}$)	^{40}Ar ($\times10^{-5}$)	$^{3}He/^{4}He$ (R_A)	$^{20}Ne/^{22}Ne$	$^{21}Ne/^{22}Ne$	$^{40}Ar/^{36}Ar$	$^{38}Ar/^{36}Ar$	$^{40}Ar^{*}$ ($\times10^{-5}$)
Qs1	4.15(12)	0.75(3)	4.8(2)	0.031(8)	9.81(3)	0.0288(4)	431(2)	0.202(5)	1.46(5)
Qs3	29.23(86)	9.36(34)	13.8(5)	0.032(2)	9.94(3)	0.0290(3)	392(2)	0.188(3)	3.29(13)
Qs4	22.24(65)	3.25(12)	5.0(2)	0.026(2)	9.81(3)	0.0290(3)	401(2)	0.190(5)	1.28(5)
Qs5	8.27(23)	1.20(4)	5.2(2)	0.030(1)	9.73(3)	0.0292(4)	497(1)	0.193(5)	2.09(8)
Qs6	0.52(2)	0.115(4)	2.3(1)	0.017(4)	9.77(3)	0.0297(3)	493(2)	0.189(4)	0.92(3)
Qs7	8.47(25)	561(20)	229(8)	0.428(20)	10.06(4)	0.0293(3)	291(3)	0.187(4)	n/a
Qs9	3.10(9)	187(7)	72(3)	0.482(7)	10.07(3)	0.0296(3)	291(1)	0.187(6)	n/a
Qs10	1.58(5)	2.86(10)	11.3(4)	na	9.82(9)	0.0285(5)	341(1)	0.186(4)	1.39(6)
Qs11	0.96(3)	2.59(9)	9.2(3)	na	9.84(3)	0.0289(2)	343(2)	0.187(8)	1.20(6)
Qs12	1.27(4)	3.46(13)	10.1(4)	0.027(3)	9.84(6)	0.0294(7)	320(2)	0.188(5)	0.68(6)
Qs14	2.55(7)	84(3)	42(2)	0.307(10)	10.08(3)	0.0296(3)	298(1)	0.190(5)	n/a
Qs15	18.30(54)	195(7)	86(3)	0.115(4)	10.04(4)	0.0295(3)	302(2)	0.185(5)	0.91(43)
Qs17	33.25(96)	na	18.8(7)	0.026(1)	na	na	368(1)	0.188(10)	3.58(14)
Qs18	2.16(6)	0.51(2)	12.5(4)	0.013(1)	9.87(3)	0.0295(3)	358(2)	0.196(4)	2.06(9)
Qs19	3.50(10)	52(2)	31(1)	0.153(3)	10.18(3)	0.0293(2)	309(1)	0.186(4)	1.06(10)
Qs20	6.38(18)	3.83(14)	12.3(4)	0.022(1)	9.69(9)	0.0289(5)	365(1)	0.196(4)	2.23(8)
Qs21	0.93(3)	0.150(6)	2.8(1)	0.023(3)	9.81(3)	0.0301(7)	451(2)	0.187(1)	0.95(4)
Qs22	2.38(7)	0.37(1)	5.2(2)	0.009(2)	9.78(3)	0.0297(4)	428(3)	0.184(8)	1.56(6)
Qs23	14.14(42)	10.54(38)	19.1(7)	0.037(2)	9.91(3)	0.0289(3)	370(3)	0.193(10)	3.71(18)
Air	5.24(5)	16.45(4)	934(1)	1.000(9)	9.80(8)	0.0290(2)	298.6(3)	0.1885(3)	

775 1σ standard deviation is shown as the last significant figures in parentheses.

776 Noble gas concentrations are in unit of cm^3 STP/cm^3 with standard conditions after Ozima and Podosek, (2002) (p =0.101 MPa, T = 0 °C).

777 Air composition is after Eberhardt et al. (1965); Györe et al. (2019); Lee et al. (2006); Mark et al. (2011); Ozima and Podosek (2002).

778 R_A is the atmospheric $^{3}He/^{4}He$ ratio of 1.34×10^{-6} (Mishima et al., 2018).

779 $^{40}Ar^{*}$ is calculated air-free ^{40}Ar.

780 na: not analysed; n/a: not applicable.